Nonlinear Dyn
https://doi.org/10.1007/s11071-018-4267-1

ORIGINAL PAPER

Nonlinear dynamic analysis of a 3D guyed mast

Jorge S. Ballaben · Marta B. Rosales

Received: 12 April 2017 / Accepted: 5 April 2018

Abstract Guyed masts are examples of structures extensively used in civil engineering. During the service life of the structure, the guys tension values can vary due to various circumstances. The consequences can range from operational difficulties to failure of the structure or some of its components. Thus, a study of the sensitivity of the dynamic response of a guyed mast to the initial pretension of the guys becomes relevant. A three-dimensional guyed mast is herein represented by a beam column and one level of three nonlinear inclined cables, with a prescribed dynamic lateral load acting on the mast. The second-order effect of the axial load due to the cables pretension on the mast is also considered. The load is designed to avoid resonance effects and meet the maximum displacement limits within the Euler–Bernoulli theory used in the beam-column model. The guys behavior is governed by cable nonlinear equations that account for the extensibility and the initial deformed configuration due to gravity. An ad hoc algorithm was developed by the authors as a tool to analyze 3D guyed masts with an arbitrary number of guys and levels of guys. The partial differential equation system is discretized using finite elements and solved in the time domain through Newmark and Newton–Raphson algorithms. A natural vibrations study shows that a single eigenvalue could be associated to local cable or mast modes or global cable–mast modes, depending on the initial pretension. The displacements of the mast at two strategic points exhibit a rich range of dynamic responses, showing different bifurcation patterns, which can turn from periodic to nonperiodic motions within small ranges of variation of the initial pretension.

Keywords Guyed mast · Nonlinearity · Dynamic response · Bifurcations

1 Introduction

Guyed masts are a structural typology extensively employed to support devices such as antennas for radio, TV and other types of telecommunication ancillaries (Fig. 1a). Its low cost offers clear advantages in the open country where there are no restrictions on the position of the cable anchors. However, nowadays it is commonly found in urban areas. Despite the large potential of adverse impact (in particular, bad quality of the signal transmission), the dynamic response is not studied in detail with exception of special cases [1–5]. On the other hand, the dynamic behavior of taut cables is widely reported in the literature (i.e., [6–8]). Other authors' works show through reduced order models (ROM), that guyed structures have special sensitivity to the type and amplitude of the excitation [9–11],

J. S. Ballaben · M. B. Rosales (✉)
Department of Engineering, Universidad Nacional del Sur and IFISUR-CONICET, Alem 1253, 8000 Bahía Blanca, Argentina
e-mail: mrosales@criba.edu.ar

J. S. Ballaben
e-mail: jorgeballaben@gmail.com

Published online: 26 April 2018

even avoiding the resonance effects. After the derivation of the equations of motion (EOM) of a cable-stayed beam, the in-plane and out-of-plane eigenvalue problems are solved by [12]. Also, nonlinear modes are studied along with the contribution of the coupling term. In recent works by the authors [13,14], the nonlinear dynamic response of a plane guyed structure is analyzed using a reduced order model considering uncertainties in structural parameters and loads. Nonlinear dynamics and bifurcation analysis are frequently conducted by means of ROM due to the computational cost and available tools.

Finite element static analysis of guyed masts is performed in [15]. The optimization of guyed structures using finite element dynamic analysis and stochastic loads is performed in [16].

In the present study and using the classical extended Hamilton's principle, the EOM that govern the vibrations of the system are obtained. Afterward, the nonlinear model of the cable follows the approach reported in [17]. Then, and after the statement of the weak form, the governing system is discretized using finite elements. The finite element method (FEM) approximation to the complete model in a dynamic nonlinear analysis is computationally expensive. In order to alleviate this cost, an ad hoc, nonlinear, optimized code for guyed structures was developed by the authors within a FEM environment. With this tool, sensitivity analysis is possible in reasonable times. The results here presented include eigenvalue and modal shape studies, in which, among other features, the veering phenomena is observed. Afterward, an uniformly distributed harmonic load is applied on the mast. The system response (displacements of the column) exhibits a variety of different dynamic behaviors which are strongly sensitive to the value of initial tension of the guys. The displacements feature bifurcations at different values of the guy tension. Both bifurcation and phase plots help to visualize these phenomena.

2 Energy formulation of columns and taut cables

The following assumptions are made: (a) both the cable and the beam column are considered as homogeneous one-dimensional elastic continua obeying a linear stress–strain relationship; (b) the initial equilibrium configuration for the inclined cable is represented by a quadratic parabola under the assumptions of small sag to length ratio; (c) axial extensions of the cable are described by the Lagrangian elongation of the centerline; (d) the flexural, torsional and shear stiffnesses of the cables are neglected; (e) the shear strain of the beam column is assumed negligible; (f) the second-order effect due to the axial load (assumed constant) is accounted for in the beam-column equation and (g) the nonlinearity of the problem arises from the cable formulation. Under these assumptions and using the classical extended Hamilton's principle, the energies governing the dynamic motions of columns and cables are obtained.

For the column

$$\delta K = \int_{t_i}^{t_{i+1}} \int_0^l m(\dot{v}\delta\dot{v} + \dot{u}\delta\dot{u} + \dot{w}\delta\dot{w})\mathrm{d}x\ \mathrm{d}t \tag{1}$$

$$\begin{aligned}\delta U = \int_{t_i}^{t_{i+1}} \int_0^l \big[&EI_z v''\delta v'' + EI_y w''\delta w'' + EAu'\delta u' \\ &+ GI_x\theta'\delta\theta' + Nv'\delta v' + Nw'\delta w'\big]\mathrm{d}x\ \mathrm{d}t,\end{aligned} \tag{2}$$

$$\begin{aligned}\delta V = \int_{t_i}^{t_{i+1}} \int_0^l &\big[q_y\delta v + q_z\delta w + q_x\delta u + q_\mathrm{T}\delta\theta\big]\mathrm{d}x \\ &+M_{z_0}\delta v_0' - M_{z_l}\delta v_l' + M_{y_0}\delta w_0' \\ &-M_{y_l}\delta w_l' - Q_{y_0}\delta v_0 + Q_{y_l}\delta v_l - Q_{z_0}\delta v_0 \\ &+Q_{z_l}\delta v_l + P_0\delta u_o - P_1\delta u_1 \\ &+T_0\delta\theta_o - T_1\delta\theta_1\ \mathrm{d}x\mathrm{d}t,\end{aligned} \tag{3}$$

By means of the extended Hamilton principle, the energy formulation governing the dynamic motions of columns is obtained by substracting potential energies Eqs. 2 and 3 to the kinetic energy Eq. 1.

$$\delta L = \delta K - (\delta U + \delta V) = 0 \tag{4}$$

For the cables

$$\delta K = \int_{t_i}^{t_{i+1}} \int_0^l m(\dot{u}\delta\dot{u} + \dot{v}\delta\dot{v} + \dot{w}\delta\dot{w})\mathrm{d}x\ \mathrm{d}t, \tag{5}$$

$$\delta U = \int_{t_i}^{t_{i+1}} \int_0^l [EA\varepsilon\delta\varepsilon + H\delta\varepsilon]\,\mathrm{d}x\ \mathrm{d}t, \tag{6}$$

$$\begin{aligned}\delta V = \int_{t_i}^{t_{i+1}} \int_0^l &\big[q_y\delta v + q_z\delta w + q_x\delta u\big]\mathrm{d}x \\ &+Q_{y_0}\delta v_0 + Q_{y_l}\delta v_l - Q_{z_0}\delta v_0 \\ &+Q_{z_l}\delta v_l + P_0\delta u_o - P_1\delta u_1\ \mathrm{d}x\ \mathrm{d}t,\end{aligned} \tag{7}$$

with:

$$\delta\varepsilon = \delta u' + Y'\delta v' + v'\delta v' + w'\delta w'. \tag{8}$$

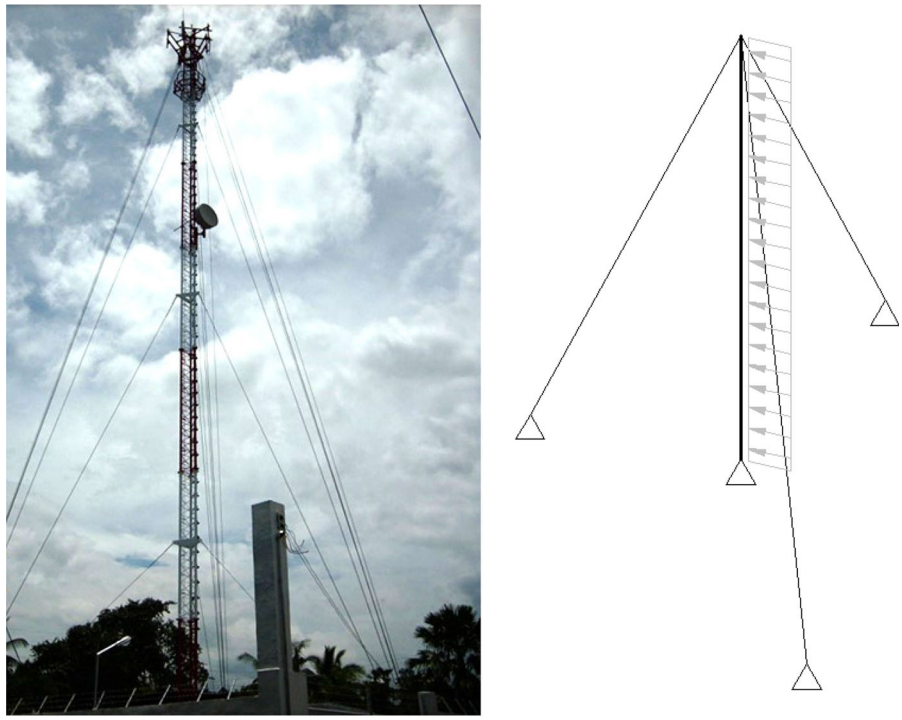

(a) **(b)**

Fig. 1 Guyed mast. **a** Typical guyed tower for mobile signal transmission; **b** model under study

Then, by introducing the Eqs. 5, 6 and 7 in Eq. 4, the energy formulation governing the motion of taut cables can be obtained.

K, U and V are the kinetic energy, the (elastic deformation) potential energy, and the work of the external loads, respectively; δ is the operator indicating the variation of a functional or function; $\dot{(*)} = \frac{\mathrm{d}(*)}{\mathrm{d}t}$; $(*)' = \frac{\mathrm{d}(*)}{\mathrm{d}x}$, u, v and w are the displacements in the axial (x) and transverse directions (y and z), respectively. θ is the gyration about the axial axis. E is the Young modulus, G is the shear modulus, I is the second-order moment of the cross section area respect to the axis indicated in the subindex, A is the cross section area, m is the mass per unit length. ε is the uniaxial Green–Lagrange elongation of the cable. H is the initial tension of the cable (in the direction of the sag). q are distributed loads in the direction corresponding to the subindex (q_T is a torsional distributed moment); Q, M, T and P are the transversal forces, and bending moments, (in the direction of the subindex) and torsional moments and axial forces, respectively, at the extremes ($x = 0$ and $x = l$) of the studied section. Y is the initial deformed configuration of the cable.

2.1 Weak formulation and finite element discretization

A general form of the weak formulation writes as

$$M(\ddot{v}, \phi) + C(\dot{v}, \phi) + K(v, \phi) + \mathrm{BC}(v, \phi) = F(v, \phi), \tag{9}$$

where M, C, F, K are the mass, damping, external force and stiffness operators, respectively. BC is the boundary condition operator. ϕ denote the admissible functions and $v = \{u, v, w, \theta\}$ for the column or $v = \{u, v, w\}$ for the cables, are solutions of the equations.

The operators for the column are:

$$\mathcal{M}(\phi, \ddot{v}) = \int_0^l \phi m\Big(\ddot{u} + \ddot{v} + \ddot{w}\Big)\mathrm{d}x, \tag{10a}$$

$$\mathcal{C}(\phi, \dot{v}) = \int_0^l \phi c\Big(\dot{u} + \dot{v} + \dot{w}\Big)\mathrm{d}x, \tag{10b}$$

$$\mathcal{F}(\phi, v) = \int_0^l \phi\Big(q_y + q_z + q_x + q_\mathrm{T}\Big)\mathrm{d}x, \tag{10c}$$

$$\mathcal{K}(\phi, v) = \int_0^l \Big(EI_z v''\phi'' + EI_y w''\phi'' + EAu'\phi' + GI_x\theta'\phi' - P_H v'\phi' - P_H w'\phi'\Big)\mathrm{d}x, \tag{10d}$$

$$\begin{aligned}\mathcal{BC} = & EI_z v'''\phi\big|_0^l + EI_y w'''\phi\big|_0^l \\ & - EI_z v''\phi'\big|_0^l - EI_y w''\phi'\big|_0^l \\ & + P_H v'\phi\big|_0^l + P_H w'\phi\big|_0^l \\ & + EAu'\phi\big|_0^l + GI_x\theta'\phi\big|_0^l \end{aligned} \tag{10e}$$

The operators for the cables are:

$$\mathcal{M}(\phi, \ddot{v}) = \int_0^l \phi m\left(\ddot{u} + \ddot{v} + \ddot{w}\right)\mathrm{d}x, \tag{11a}$$

$$\mathcal{C}(\phi, \dot{v}) = \int_0^l \phi c\left(\dot{u} + \dot{v} + \dot{w}\right)\mathrm{d}x, \tag{11b}$$

$$\mathcal{F}(\phi, v) = \int_0^l \phi\left(q_x + q_y + q_z\right)\mathrm{d}x, \tag{11c}$$

$$\begin{aligned}\mathcal{K}(\phi, v) = & \int_0^l \left[\phi' H v' + \phi' H w'\right. \\ & + \phi' EA(Y' + v')\left(u' + Y'v' + \frac{v'^2}{2} + \frac{w'^2}{2}\right) \\ & \left. + \phi' EA\left(u' + Y'v' + \frac{v'^2}{2} + \frac{w'^2}{2}\right)\right]\mathrm{d}x, \end{aligned} \tag{11d}$$

$$\begin{aligned}\mathcal{BC} = & Hv'\phi\big|_0^l + Hw'\phi\big|_0^l + EA(Y' + v') \\ & \left(u' + Y'v' + \frac{v'^2}{2} + \frac{w'^2}{2}\right)\phi\big|_0^l \\ & + EA\left(u' + Y'v' + \frac{v'^2}{2} + \frac{w'^2}{2}\right)\phi\big|_0^l \end{aligned} \tag{11e}$$

After stating the weak formulation, the system is discretized by means of an ad hoc nonlinear finite element (NLFEM) formulation. The column is modeled using two nodes, 6-DOF (transverse and axial displacements and slope at each node) beam element (Hermite interpolation functions for the transverse displacements and their derivatives and linear interpolation functions for the axial displacements and the torsional rotations) and the cable using a three nodes, 6-DOF (axial and transverse displacements at each node) cable element (quadratic interpolation functions). The nonlinear dynamic response is obtained using the Newton–Raphson method for the iterations and the Newmark method for the time integration. As an initialization and before the dynamic run, the pretension of the guys is applied through a deformation of the cables (step 1); then, the self-weight of the guys is activated (step 2). Figure 2a shows an scheme of the guyed mast geometry. Steps 1 and 2 are depicted in Fig. 2b, c. The position of the anchors and the initial pretension are checked (step 3). If the error is less than 0.5%, the program uses this deformed/stressed state as the initial state of the dynamic analysis. Otherwise, the initial length of the cable is modified (step 4) and steps 1–4 are repeated until the error meets the prescribed tolerance.

To improve the runtime, the initial configurations as well as rotation, mass and linear stiffness matrices were first solved and preallocated. Thus, the solver only needs to recalculate the linearized stiffness matrix of the cable elements and the residual vectors at each iteration. Also, a parallelization of the algorithm is implemented.

2.2 Numerical illustration

The studied problem consists in a 20 m height guyed mast, as depicted in Fig. 2a, with one level of three cables at the top. The anchors of the cables are separated 10 m from the mast and 120° of each other. The mast is fixed at the base and is modeled using 5 beam elements with consideration of the second-order effect. The cables are pinned at the anchor point and each cable is discretized with 5 three-node nonlinear cable elements. The dynamic load (designed to obtain maximum column displacements within the limits of the Bernoulli beam theory) is applied on the mast and consists in a uniformly distributed load of 400 N, with a time variation given by $f(t) = 0.5\cos(3\pi t) + 1.1$. The assumed values of the constants are: $E = 209$ MPa, $I_x = I_y = 3 \times 10^{-5}$ m^4, $I_z = 6 \times 10^{-5}$ m^4, $A_b = 1.5 \times 10^{-3}$ m^2, $m_b = 11.77$ kg/m, $A_c = 7.85 \times 10^{-5}$ m^2, $m_c = 0.62$ kg/m and $H = 1000$–$13{,}500$ N.

3 Results

3.1 Natural frequency analysis

The stiffness matrix of the elements is computed using the initial deformed shape. The reduction of the stiffness of the column due to the tension components of the guys is also considered. In Fig. 3, the evolution of some of the natural frequencies with the tension is depicted. The excluded curves represent small variations of the ones depicted and are avoided in order to make the plot clearer. The nonlinear evolution of each eigenvalue with H is apparent, and it is a consequence of the nonlinear formulation of the cables.

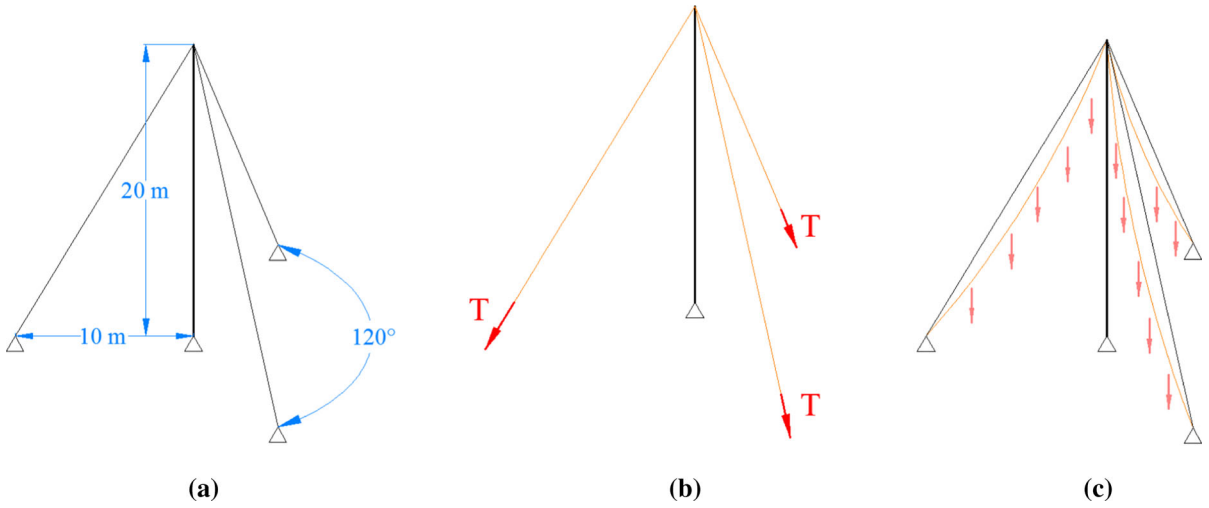

Fig. 2 Geometry of the studied guyed mast and first two steps to get the initial deformed/stressed configuration for the dynamic/uncertainty studies. **a** Guyed mast geometry. **b** Step 1: cables pretension. **c** Step 2: cables self-weight

Fig. 3 Eigenvalues evolution with the initial tension

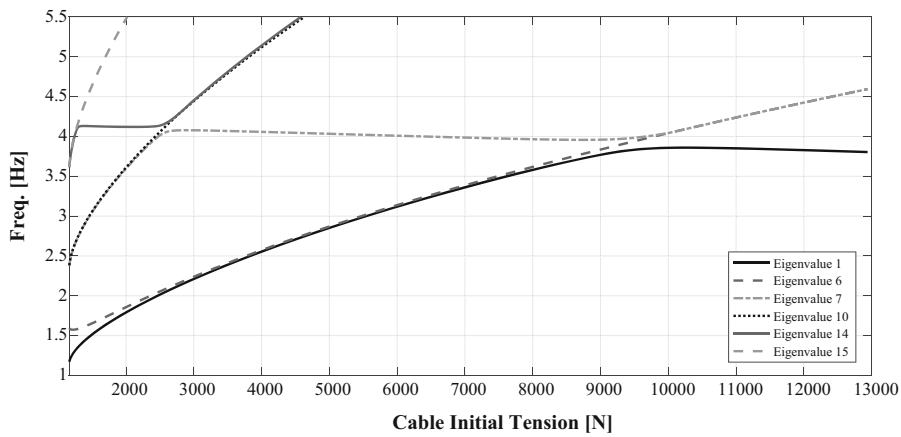

In some cases, the curves become parallel and close, though no crossings are observed. At some values of the initial tension, rapid changes (with respect to the previous rate) in the derivative of the curves occur. In these zones, the veering phenomena is observed and the mode shape associated to a given eigenvalue starts to change gradually, in general, from a local (cable or column) shape to a global cable–column shape. Then, when the changes in the derivative slow down, the modal shape becomes local again. An example of this process is illustrated in Fig. 4: the evolution of two eigenvalues with the cable initial tension where the veering phenomena is observed, is shown at the top plot; the local and global modal shapes associated with certain ranges of H are depicted with different line patterns. The distinction between a local and a global modal shape is performed using the so-called localization factor [7]:

$$\Lambda_{i,j} = \frac{(\mathbf{R}_j\phi_i)^{\mathrm{T}}\mathbf{M}(\mathbf{R}_j\phi_i)}{\phi_i^T\mathbf{M}\phi_i}; \quad \Lambda_{i,j} \in [0,1] \tag{12}$$

where ϕ_i is the ith eigenvector and $\mathbf{M}$ is the mass matrix of the model while $\mathbf{R}_j$ is a diagonal matrix of ones and zeroes that allows a selection of the degrees of freedom along the cables. The $\Lambda_{i,j}$ factor expresses the localization level of the ith eigenvector in the jth cable domain. Clearly, $\Lambda_{i,j} = 0$ corresponds to a local cable modal shape and $\Lambda_{i,j} = 1$ to a local column modal shape. When $0 < \Lambda_{i,j} < 1$, a hybrid cable–column modal shape is present. In Fig. 4 (bottom), the different modal shapes associated with the corresponding eigenvalue and range of H are depicted. Here, a smooth but

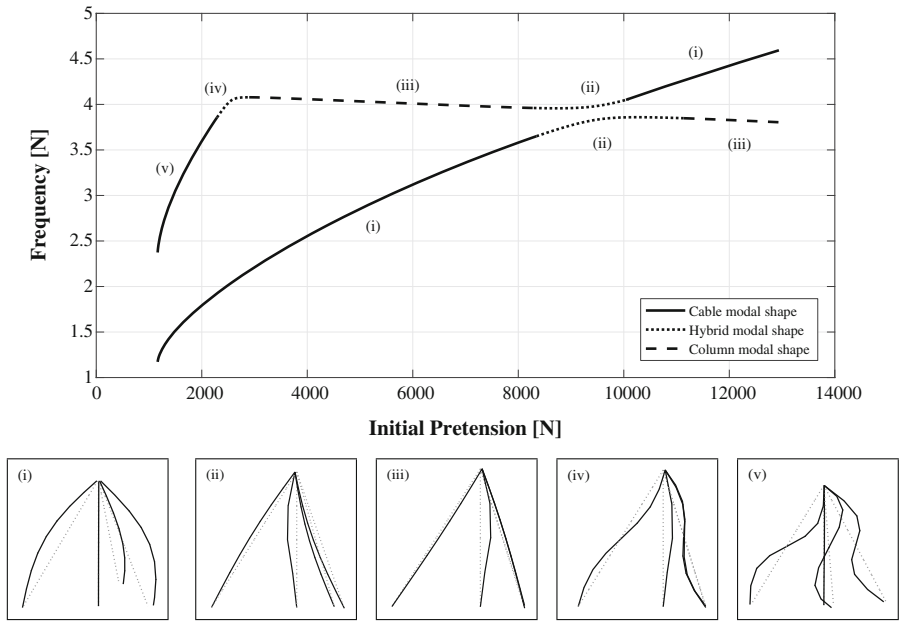

Fig. 4 Hybridization of modal shapes and veering of eigenvalues: evolution with the initial tension and veering of eigenvalues (top) and modal shapes associated with the eigenvalues (bottom)

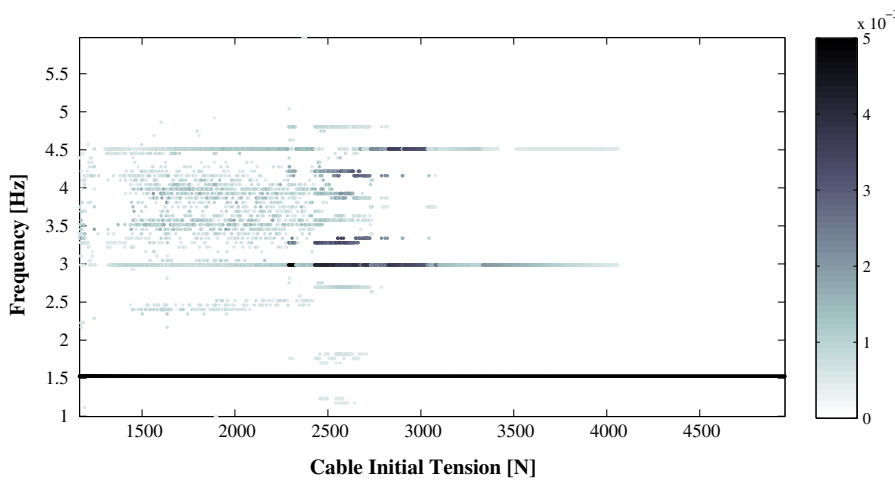

Fig. 5 Peaks of FFT of top displacements: evolution with the cable initial tension

rapid transition between a local (i.e., cable or column) mode to other local shape (i.e., column or cable, respectively) corresponds to the hybridization of the mode shapes. Also, the hybridization regions correspond to the veering zones, where an exchange of local modal shapes occurs between the eigenvalues (as can be seen in Fig. 4 top for $H \approx 9500\,\text{N}$). The hybrid shapes are rare (are apparent in small ranges of H) probably due to the difference in the stiffness between the cables and the column.

Additionally, a decrease in the frequency is observed in particular ranges of H (i.e., mode 1, $H = 11{,}000$: 13,500 N or mode 7, $H = 3000$:9000 N), for increasingly higher values of H. This effect always happens in local column modes and it is a consequence of the second-order effect, which leads to a reduction in the column stiffness, proportional to the initial tension of the guys. If the second-order effect is neglected, this particularity is lost.

3.2 Guyed mast under dynamic load

Regarding the behavior of the structure under dynamic loading, the displacements at the top of the mast in the load direction are herein presented. A Fast Fourier

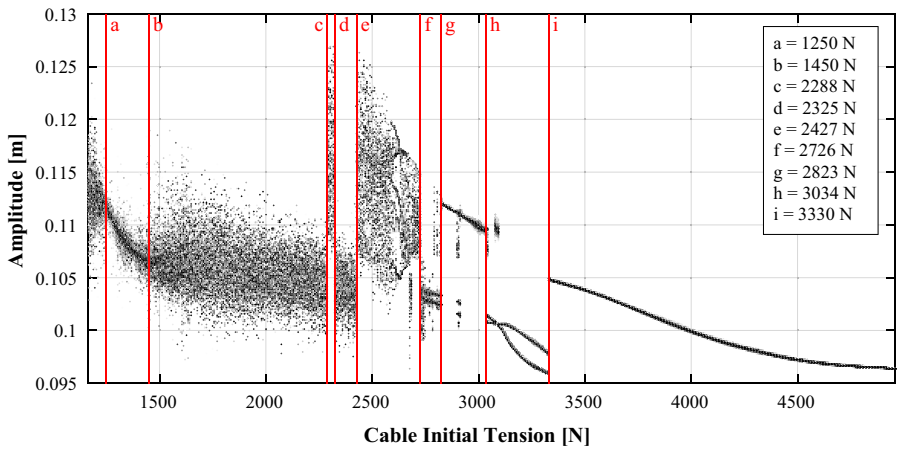

Fig. 6 Bifurcation diagram of the Poincare map

Transform (FFT) study (Fig. 5) shows that the main frequency of vibration is 1.5 Hz and matches the load frequency. Other less important components can be observable depending on the cable initial tension. The first (3 Hz) and second (4.5 Hz) superharmonic frequencies are present in the most of the cases with $H < 4000$ N. Also, the range of $H < 2800$ N exhibits, in general, a myriad of peaks of small importance, which may indicate a nonperiodic or chaotic behavior.

The displacements exhibit a highly sensitive dependence on the value of cable initial tension, affecting both the amplitude and the dynamic response. In Fig. 6, a bifurcation plot of the Poincaré map is depicted (the sampling time corresponds to the load frequency). The dots are colored from light gray to black, so the darkest are the latest dots sampled. Since this is a numerical study with a finite time span, by this means, some attractor trends can be easily identified, even when the time span studied may not be enough to fully stabilize the dynamics. The zones delimited by the vertical lines, indicated with lower-case letters a to i in Fig. 6, seem to present a common attractor, except for the zone e to f. The lines c to i also point out the values of initial pretension that lead to abrupt bifurcations in the dynamic behavior. In the Figs. 8, 9 and 10, the characteristic zones of the bifurcation diagram are isolated and the attractors are depicted with the help of partial state space plots (force vs displacement and force vs velocity).

The periodicity ratio (PR) [18,19] is also computed and illustrated in Fig. 7. This parameter, which is calculated starting from the Poincaré map, allows to classify the dynamic of a signal from periodic (PR = 1) to non-periodic and potentially chaotic (PR = 0) and all the intermediate cases.

The range of values where the nonlinearity of the guys becomes more relevant ($H \in$ [1450:3300]) includes both potentially chaotic and periodic responses. The region of Fig. 6 with a disperse set of points with no clear trend (e.g., $H = 2000$ N) can be an indicator of aperiodic or chaotic motion (within the studied time span). The behaviors observed for each value of H in Fig. 6 can be classified—or confirmed—with the aid of Fig. 7. Also, the point to point variability observed of Fig. 7 gives further insights of the high sensitivity of the structure to the values of initial tension H. There are four characteristic zones in the periodicity ratio diagram of Fig. 7: (1) $H \in$ [1200:1450], where $0.2 < \text{PR} < 0.95$. In this zone, the cables are slack and the system works as a fixed-free beam. Within this range of H, the cables offer no support to the mast and just add nonlinear noise to the dynamic response. (2) $H \in$ [1450:2726], where $0 < \text{PR} < 0.2$. The nonlinear influence of the cables becomes apparent and the dynamic behavior of the structural system is complex and frequently aperiodic. (3)$H \in$ [2726:3330], where $0.2 < \text{PR} < 0.95$. This zone is a transition zone: the system response moves to more periodic solutions through the increase of H, while the nonlinearity tends to decrease (4)$H \in$ [3330:5000], where $0.8 < \text{PR} < 1$. In this zone, the dynamic response has a clear periodic attractor (as can be seen in Fig. 6): the nonlinear effect of the cables is rapidly lost due to the high initial tension.

Next, the bifurcation diagram is discussed in detail. In Fig. 8, the zones within lines a to b and b to d of Fig. 6

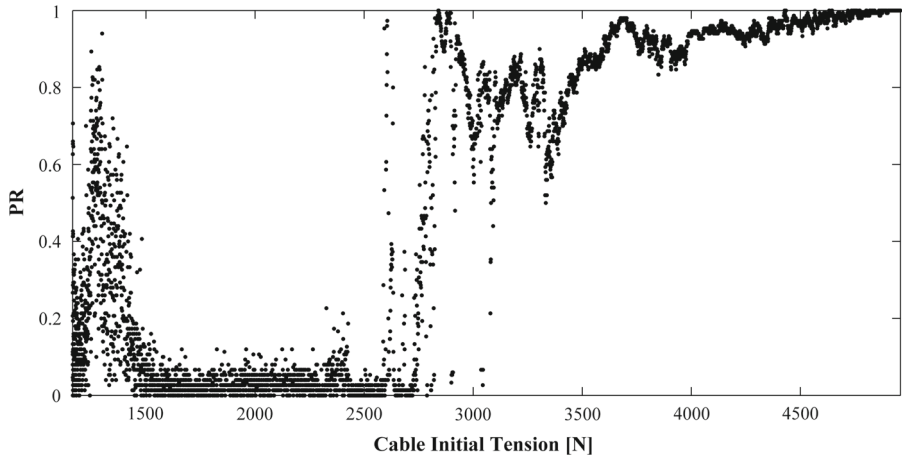

Fig. 7 Periodicity ratio of top displacements evolution with the cable initial tension

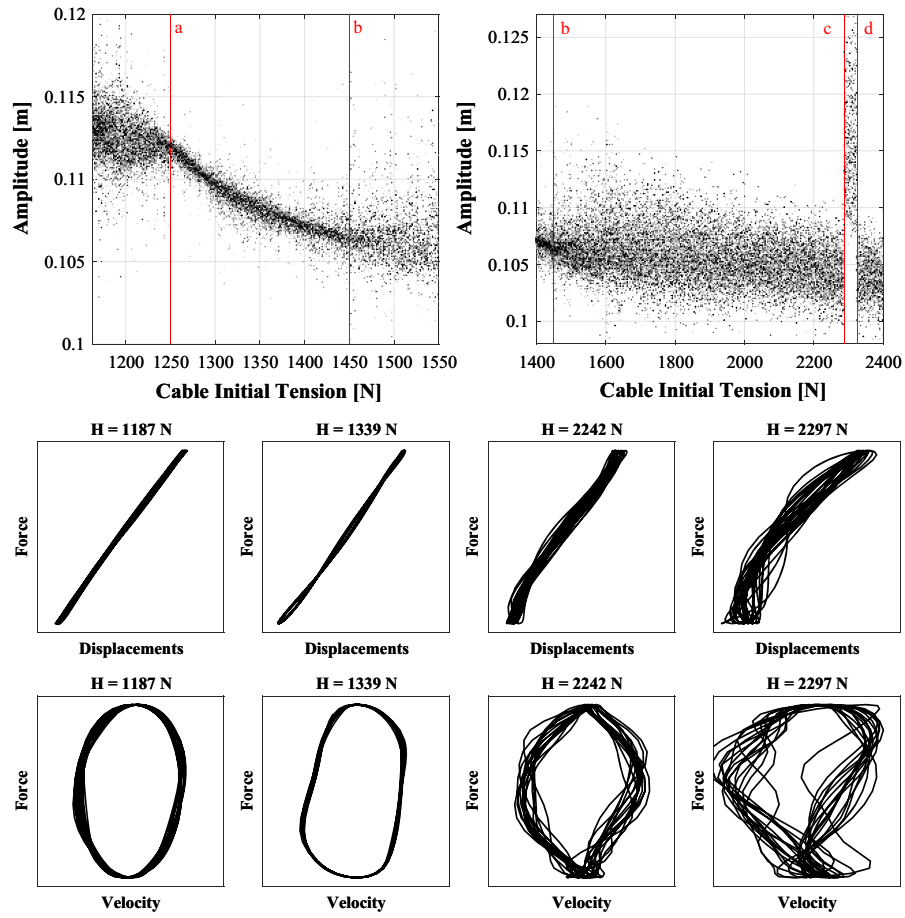

Fig. 8 Top: details of the bifurcation diagram (Fig 6), zones within lines a to b and b to d, respectively. Small bottom figures: partial space state plots (force vs displacement and force vs velocity) depicting the attractors observed within the zones limited by the lines

are enlarged and space state plots which depict the characteristic attractor within each zone are included. For the loosest cases ($H < b$) the system tends (approximately) to a plane ellipse in the space state, but the PR indicates that just a handful of cases could be cataloged as periodic, since $0.2 < \mathrm{PR} < 0.95$. The observation of Fig. 8 (top left) suggests a periodic attractor, but a longest time span would be necessary to soundly support this statement. For the loosest cases, it seems that the main vibration behavior is due to the interaction

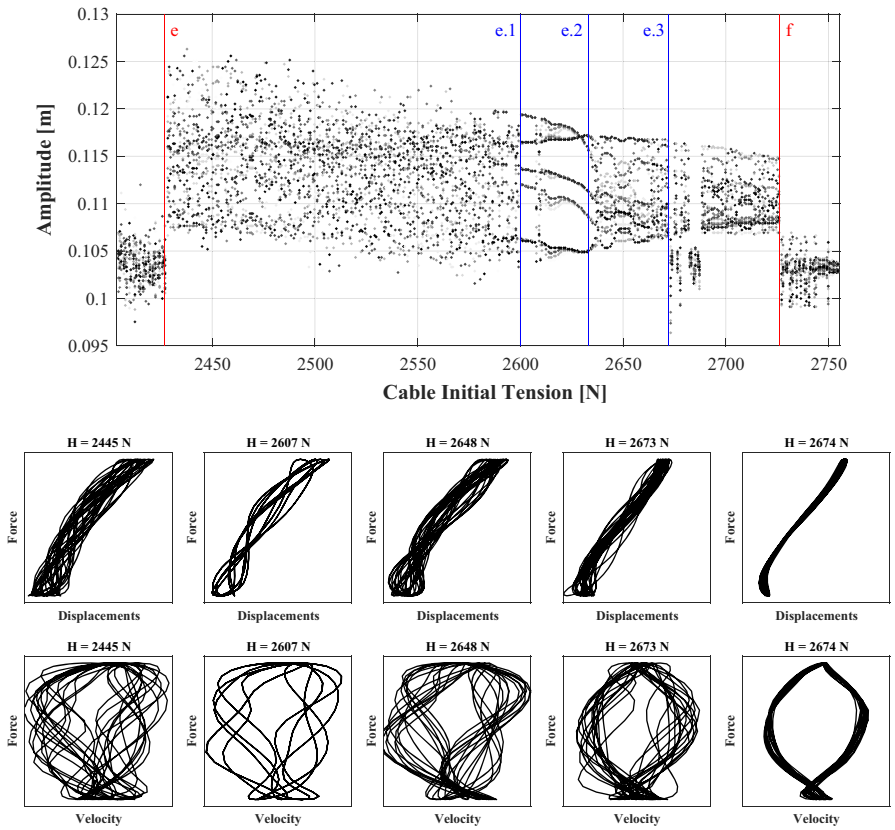

Fig. 9 Top: details of the bifurcation diagram (Fig 6), zones within lines d to f. Small bottom figures: partial space state plots (force vs displacement and force vs velocity) depicting the attractors observed within the zones limited by the lines

of the column load and the presence of the cables just adds a nonlinear noise to the displacements. In the zone where $b < H < c$, the nonlinear behavior of the cables becomes more apparent. This is observed in the space state as an increasingly more complex (and deformed) attractor, no longer contained in a plane ($H = 2242$ N), together with values of PR < 0.2. When H reaches the value of 2288 N (line c), there is an abrupt bifurcation of period 2 of the previous—mostly aperiodic—attractor. This affirmation is supported by the observation of the FFT (Fig. 5), where the peak of the of 3 Hz superharmonic equals the energy of the 1.5 Hz peak (frequency of the load) in the zone $c < H < d$. Also, the rich frequency content together with the low PR values confirm the aperiodic characteristics of the dynamics. This attractor (for $c < H < d$) comes up frequently with slight variations, as it can be seen in the following analysis, and will be named $A0$. For $d < H < e$, the attractor of the zone $b < H < c$ is recovered.

In Fig. 9, the zones within lines e to f of Fig. 6 are enlarged and space state plots which depicts the characteristic attractor within each zone are included. When H attains the line "e" (2427 N), a bifurcation similar to the one observed in the line "c", is observed. The corresponding attractor in the zone $e < H < e.1$ (i.e., for $H = 2445$ N) is also analogous to $A0$. In general, when discontinuities are observed within a given behavior (or zone) in the bifurcation diagram, they correspond with the emergence of an akin variant of $A0$. When H is close to $e.1$, the periodicity ratio starts to show higher values, and when H reaches $e.1$ ($e.1 < H < e.2$) PR > 0.8, which indicates a periodic behavior. The space state plots show a complex period-5 attractor ($H = 2607$ N), that shares various features in the space state with the previous aperiodic one. The periodic window extends up to $H = e.2$, where a variant of $A0$ is obtained (see $H = 2648$ N) for $e.2 < H < e.3$. For $e.3 < H < f$, the attractor is similar to the one in the zone $b < H < c$ (see $H = 2673$ N), and presents some small windows where it is flatter and thinner and much more periodic (see $H = 2674$ N) in terms of the PR value.

In Fig. 10, the zones within lines f to h and h to i of Fig. 6 are zoomed and space state plots which

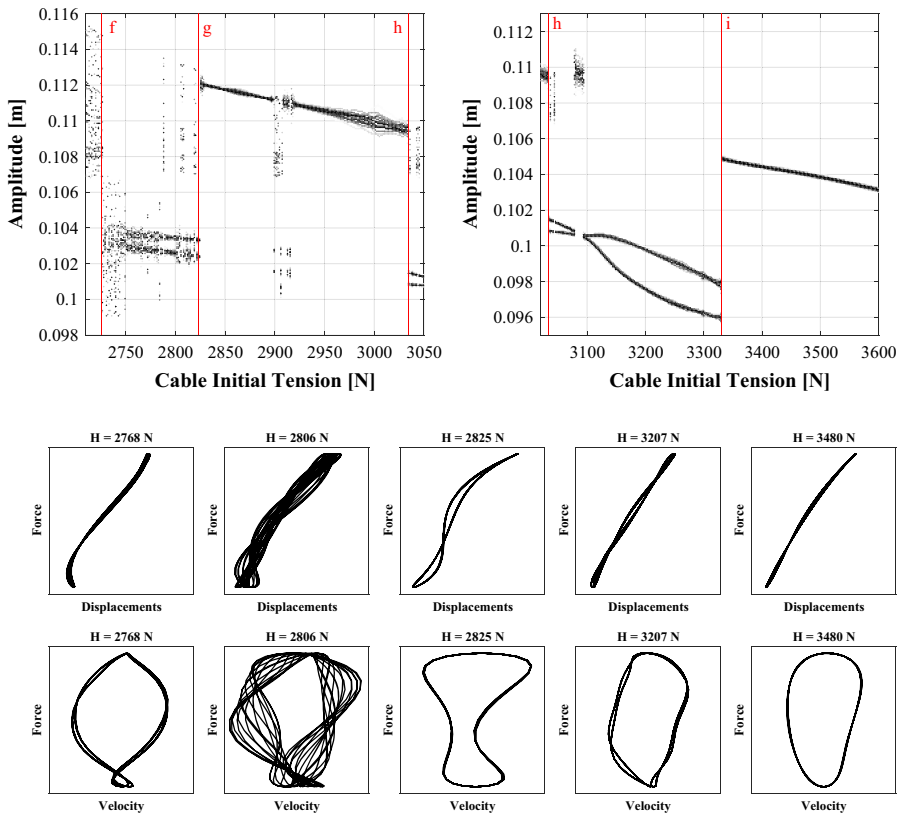

Fig. 10 Top: details of the bifurcation diagram (Fig 6), zones within lines f to h and h to i, respectively. Small bottom figures: partial space state plots (force vs displacement and force vs velocity) depicting the attractors observed within the zones limited by the lines

depict the characteristic attractors within each zone are included, as before. The whole zone starting from $H =$ f to 5000 N shows a periodic behavior (PR > 0.85 in most cases). The windows of mostly aperiodic behavior (PR < 0.2) that can be found, correspond to the variant of attractor $A0$ depicted for $H = 2806$ N in Fig. 10. The dynamic observed within the zone $f < H < g$ is depicted for $H = 2768$ N: it is a period-2 attractor with a flat profile in the space state. When H attains the value corresponding to line g, another abrupt bifurcation occurs, again augmenting the displacements and velocities, but the attractor is periodic, with period-1, and it is active for $g < H < h$. This attractor changes without transition for $H = h$, to the period-2 attractor depicted for $H = 3207$ N. Within the zone $h < H < i$, there is a bifurcation from period-2 to period-1, a mostly periodic window with a period-1 variant of the attractor and another period-2 bifurcation. When H hits the value of 3330 N, a period-1 attractor (see $H = 3480$ N) with higher displacements is obtained without transition. This last attractor is maintained, reducing its size when H is increased, for all $H > i$.

4 Conclusions

The dynamic properties (natural frequencies and modes) and the dynamic response (in terms of top displacements) of a 3D guyed mast, for a wide range of values of initial pretension of the guys, were studied. To achieve this goal, a nonlinear 3D finite element formulation was stated, implemented and optimized.

Regarding the eigenvalues studies, the veering phenomenon is observed and the regions of veering correspond to transition zones (which exhibit hybrid—column and cable—modes) between local—column or cable—modes. The so-called localization factor is employed to distinct local from hybrid modes. Also, due to the influence of the second-order effect, a reduction in the natural frequency occurs (for increasing values of H) for local column modal shapes.

When the displacement of the column response to a dynamic load is studied, the main frequency of vibration equals the frequency of the load. Also, the FFT study shows the presence of other frequencies, including superharmonics of the main frequency. A variety of different dynamic behaviors are observed depend-

ing on the value of H, from single period oscillations to strange chaotic attractors. Figures of the bifurcation diagram, space state plots and the periodicity ratio are used to perform a detailed description and classification of the different types of the found dynamic behaviors. An important remark is that the rich dynamic panorama is obtained from a 3D nonlinear finite element model of the complete system (with 80 degrees of freedom), with parameter values within the range of engineering use and recommendations. Studies of this depth, on complete systems and with real-life parameter values, are not frequent in the literature. Also, the combined use of modern tools like the periodicity ratio, the localization factor or the time color gradient in the bifurcation diagram constitute a novel approach.

The results here presented allow to a better understanding of the complexity and behavior of real-life guyed masts. Future works on this model could include the variation of amplitude, frequency and direction of the load, consideration of stochastic wind load, guys with different tension and/or stochastic tension or the study of the dynamics during the breakage of a guy.

Acknowledgements The authors acknowledge the financial support from CONICET, MINCyT and UNS (Argentina).

References

1. Preidikman, S., Massa, J., Roccia, B.: Análisis dinámico de mástiles arriostrados. Rev. Int. de Desastres Naturales Accidentes e Infraestructura Civil **6**, 85–102 (2006)
2. Shi, H.: Nonlinear Finite Element Modeling and Characterization of Guyed Towers Under Severe Loading. Ph.D. thesis, University of Missouri, Columbia (2007)
3. de Oliveira, M .I., da Silva, J .G., Vellasco, P .C.da S, de Andrade, S .A., de Lima, L .R.: Structural analysis of guyed steel telecommunication towers for radio antennas. J. Braz. Soc. Mech. Sci. Eng. **29**, 185–195 (2007)
4. Saudi, G.: Structural assessment of a guyed mast through measurement of natural frequencies. Eng. Struct. **59**, 104–112 (2014)
5. Shi, H., Salim, H.: Geometric nonlinear static and dynamic analysis of guyed towers using fully nonlinear element formulations. Eng. Struct. **99**, 492–501 (2015)
6. Babaz, M., Jezequel, L., Lamarque, C.-H., Perrard, P.: Unusual expression of tension of a massless cable with application to the oscillations of a mass suspended to a cable with a variable length. J. Sound Vib. **363**, 446–459 (2016)
7. Gattulli, V., Martinelli, L., Perotti, F., Vestroni, F.: Dynamics of suspended cables under turbulence loading: reduced models of wind field and mechanical system. J. Wind Eng. Ind. Aerodyn. **95**, 183–207 (2007)
8. Macdonald, J.: Multi-modal vibration amplitudes of taut inclined cables due to direct and/or parametric excitation. J. Sound Vib. **363**, 473–494 (2016)
9. Lenci, S., Ruzziconi, L.: Nonlinear phenomena in the single mode dynamics of a cable-supported beam. Int. J. Bifurcat. Chaos **19**, 923–945 (2009)
10. Wei, M.H., Xiao, Y.Q., Liu, H.T.: Bifurcation and chaos of a cable–beam coupled system under simultaneous internal and external resonances. Nonlinear Dyn. **67**, 1969–1984 (2011)
11. Wei, M., Lin, K., Jin, L., Zou, D.: Nonlinear dynamics of a cable-stayed beam driven by sub-harmonic and principal parametric resonance. Int. J. Mech. Sci. **110**, 78–93 (2016)
12. Wang, Z., Sun, C., Zhao, Y., Yi, Z.: Modeling and nonlinear modal characteristics of the cable-stayed beam. Eur. J. Mech. A Solids **47**, 58–69 (2014)
13. Ballaben, J.S., Rosales, M., Sampaio, R.: Stochastic dynamics of a non-linear cable-beam system. J. Braz. Soc. Mech. Sci. Eng. **38**, 307–316 (2016)
14. Ballaben, J.S., Sampaio, R., Rosales, M.B.: Uncertainty quantification in the dynamics of a guyed mast subjected to wind load. Eng. Struct. **132**, 456–470 (2017)
15. Pezo, M., Bakic, V., Markovic, Z.: Structural analysis of guyed mast exposed to wind action. Therm. Sci. **20**, 1473–1483 (2016)
16. Venanzi, I., Materazzi, A.L., Ierimonti, L.: Robust and reliable optimization of wind-excited cable-stayed masts. J. Wind Eng. Ind. Aerodyn. **147**, 368–379 (2015)
17. Gattulli, V., Lepidi, M.: Localization and veering in the dynamics of cable-stayed bridges. Comput. Struct. **85**, 1661–1678 (2007)
18. Huang, T., Dai, L., Zhang, H.: An approach combining periodicity ratio and secondary Poincaré map for characteristics diagnosis of nonlinear oscillatory systems. Nonlinear Dyn. **84**, 959–975 (2016)
19. Dai, L.: Nonlinear Dynamics of Piecewise Constant Systems and Implementation of Piecewise Constant Arguments, 1st edn. World Scientific, Singapore (2008)